processes

MDPI

Article

Fe-Based Ternary Geopolymer Pervious Subgrade Material: Mechanical Performance, Reaction Mechanism, and Sustainability Assessment

Xian Wu [1,2], Zhan Chen [2], Xian Zhou [3], Yinhang Xu [1], Zhen Hu [4] and Zheng Fang [2,*]

[1] Wuhan Municipal Engineering Design & Research Institute Co., Ltd., Wuhan 430023, China; xuanwu@whu.edu.cn (X.W.); yhxu18908655420@163.com (Y.X.)
[2] School of Civil Engineering, Wuhan University, Wuhan 430072, China; czhuan@whu.edu.cn
[3] Research Center of Water Engineering Safety and Disaster Prevention of Ministry of Water Resources, Changjiang River Scientific Research Institute, Wuhan 430010, China; zhouxian@whu.edu.cn
[4] Institute of Advanced Studies, China University of Geosciences, Wuhan 430078, China; ahuzhen@126.com
* Correspondence: zfang@whu.edu.cn

Abstract

This study develops a ternary Fe-based geopolymer system composed of metakaolin (MK), red mud (RM), and fly ash (FA) for the preparation of sustainable water-retaining subgrade materials for sponge-city roadbed applications. Unlike conventional formulations primarily designed for structural strength or rapid permeability, the proposed MK–FA–RM system was designed to improve water-storage capacity while maintaining adequate mechanical support and environmental compatibility. In this ternary system, MK provides highly reactive aluminosilicate species for geopolymer network formation, RM introduces Fe-bearing phases and enhances industrial solid-waste utilization, and FA contributes to particle packing, workability, and resource efficiency. A constrained ternary mixture design implemented using Design-Expert software was adopted to optimize precursor proportions. Within the investigated compositional range, the fitted first-order mixture model showed acceptable statistical adequacy for preliminary composition screening (R^2 = 0.86). The optimal blend (60% MK, 30% RM, and 10% FA) achieved a 7-day compressive strength of 8.37 MPa and a water retention rate of 35.3% under ambient curing conditions, satisfying the strength requirement considered for the target subgrade/base-layer application. Microstructural and phase analyses suggest that the synergistic interaction of the three precursors promoted Fe-modified aluminosilicate gel formation together with conventional geopolymer gel products, while improving matrix continuity and preserving interconnected pore space for water storage. This multiscale structural effect helps explain how the material achieved a balance between water retention capacity and mechanical support. Under the tested conditions, the material maintained acceptable residual strength after short-term exposure to water, acid, and sulfate-containing solutions. Life-cycle assessment indicated a 70% reduction in CO_2 emissions compared with ordinary Portland cement, while pilot-scale cost analysis showed a 39% lower production cost than MetaMax-based geopolymer materials. Pilot-scale application further demonstrated the constructability and water-regulation potential of the material in practical environments. Overall, the proposed ternary Fe-based geopolymer demonstrates that Fe-rich industrial wastes can be engineered into low-carbon and economically viable water-retaining subgrade materials that balance hydraulic regulation, structural adequacy, and sustainability. Nevertheless, long-term durability, cyclic loading performance, and direct nanoscale characterization of Fe-bearing gel evolution still require further investigation.

Check for updates

Academic Editors: Shengyong Lu and Antônio Benjamim Mapossa

Received: 6 April 2026
Revised: 27 April 2026
Accepted: 13 May 2026
Published: 15 May 2026

Copyright: © 2026 by the authors. Licensee MDPI, Basel, Switzerland. This article is an open access article distributed under the terms and conditions of the Creative Commons Attribution (CC BY) license.

Keywords: geopolymer; water-retaining subgrade material; red mud; solid waste utilization; sponge city

1. Introduction

The growing urgency of climate change mitigation and resource conservation is accelerating the transition toward sustainable construction materials. Ordinary Portland cement (OPC), despite its widespread use, remains a major contributor to anthropogenic CO_2 emissions, because of its energy-intensive production and calcination processes, accounting for nearly 7% of global emissions [1]. In contrast, geopolymers and other alkali-activated aluminosilicate binders are increasingly regarded as promising low-carbon alternatives because they can reduce carbon emissions, utilize industrial by-products, and provide good durability for infrastructure applications [2–4].

A particularly attractive strategy is the use of aluminosilicate precursors and iron-rich industrial residues, especially red mud (RM), fly ash (FA), and metakaolin (MK), in alkali-activated systems. RM and FA are produced in large quantities and pose persistent environmental and disposal challenges, whereas MK serves as a highly reactive aluminosilicate precursor that can compensate for the limited reactivity of some waste-derived components [5–7]. Incorporating these materials into geopolymer matrices not only alleviates waste-disposal pressure and associated environmental risks, but also enables the production of value-added construction materials [3,5]. Among them, RM is particularly noteworthy because, as a by-product of alumina refining, it is highly alkaline, chemically complex, and rich in Fe-bearing phases. When properly incorporated into alkali-activated matrices, RM can contribute not only to waste stabilization and immobilization of hazardous species, but also to matrix formation and structural evolution, making it especially attractive for the development of sustainable functional infrastructure materials [4,8].

Nevertheless, the direct use of iron-bearing residues in alkali-activated systems remains challenging because inert or weakly reactive phases may hinder precursor dissolution, reduce gel formation efficiency, and impair matrix continuity under ambient curing conditions [2]. To overcome these limitations, recent studies have increasingly adopted multi-source precursor strategies, in which highly reactive MK is combined with lower-reactivity industrial residues such as RM and FA to improve reaction synergy, compositional balance, and microstructural development [9,10]. Such synergistic design is particularly important when the target application is not high-strength structural concrete, but water-retaining functional infrastructure materials that require a balance among water retention capacity, sufficient mechanical support, and durability under service conditions [11].

Among such applications, sponge-city road systems place particularly high demands on water-retaining subgrade materials, which are expected not only to provide basic structural support, but also to participate in stormwater regulation through water storage, drainage, and moisture exchange [11,12]. Compared with conventional dense roadbed materials, water-retaining subgrade materials with interconnected pore structures can help alleviate surface runoff, delay peak discharge, and improve the local hydrothermal environment. However, increasing pore volume for water storage often weakens load-bearing continuity and interfacial integrity, resulting in a trade-off between hydraulic functionality and mechanical performance [13,14]. Therefore, the development of water-retaining subgrade materials requires not only appropriate precursor design and pore-structure regulation, but also sufficient durability to ensure stable service under variable environmental conditions [13]. To address these challenges, this study proposes a novel ternary Fe-based geopolymer system based on MK, FA, and RM for the development of

sustainable water-retaining subgrade materials for sponge-city road applications. The study focuses on achieving a coordinated balance among water retention capacity, mechanical support, short-term service stability, and sustainability, rather than simply maximizing strength or permeability. A constrained ternary mixture design implemented using Design-Expert software was employed to optimize precursor proportions and evaluate the role of each component in the multi-source system. In addition, the effects of aggregate particle size on the balance between water retention performance and mechanical properties were investigated, and the short-term durability, pilot-scale constructability, direct cost, and carbon-emission performance of the optimized material were further assessed. Through this integrated framework, the study aims to verify the feasibility of utilizing Fe-rich industrial wastes in low-carbon water-retaining subgrade materials and to provide both mechanistic insight and engineering evidence for their practical application.

2. Materials and Methods

2.1. Raw Materials

All precursor materials used in this study were obtained from domestic suppliers in China and consisted of two industrial residues, fly ash (FA) and red mud (RM), together with one highly reactive aluminosilicate precursor, metakaolin (MK). FA and RM were supplied by Yantai Anda Environmental Protection Technology Co., Ltd. (Yantai, Shandong, China). The FA was a by-product of coal combustion, whereas the RM was generated from the Bayer process of alumina extraction. Both materials were used in their as-received condition without further treatment. The MK was produced from coal-series kaolinitic clay sourced from Xingtang County (Shijiazhuang, Hebei, China). After calcination, the MK exhibited high aluminosilicate reactivity under alkali activation and served as the main reactive precursor in the ternary system. In this study, MK was primarily used to provide a highly reactive aluminosilicate framework, RM supplied Fe-bearing components and contributed to industrial-waste utilization, and FA helped improve particle packing and resource efficiency. The chemical compositions of the three precursor materials, determined by X-ray fluorescence (XRF), are listed in Table 1, and their particle size distributions are shown in Figure 1. The alkaline activator solution was prepared by combining sodium hydroxide (NaOH) and sodium silicate (Na_2SiO_3). Analytical-grade sodium hydroxide (purity $\geq$ 96%) was supplied by Shanghai Sinopharm Chemical Reagent Co., Ltd., while sodium silicate (8.5 wt% Na_2O, 26.5 wt% SiO_2) was obtained from Bengbu Sincere Chemical Co., Ltd., Bengbu, China. The activator solution was prepared by dissolving NaOH pellets in deionized water, cooling the solution to ambient temperature, and then mixing it with sodium silicate. Crushed natural stone aggregates were supplied by Hebei Qianli Mining Co., Ltd., Hengshui, China. They were sieved into specific size fractions according to experimental requirements and stored under dry conditions. Aggregate particle size was selected as an important structural variable because of its influence on water retention performance, pore connectivity, and mechanical strength.

Table 1. Chemical compositions of the precursor materials determined by XRF.

	SiO_2	Al_2O_3	Fe_2O_3	Na_2O	CaO	TiO_2	SO_3	K_2O
RM	15.12%	27.78%	35.82%	12.01%	1.89%	5.96%	0.51%	0.10%
MK	51.58%	43.80%	2.22%	-	0.40%	1.43%	0.28%	0.29%
FA	41.96%	26.81%	13.85%	0.38%	9.34%	1.77%	1.75%	1.63%

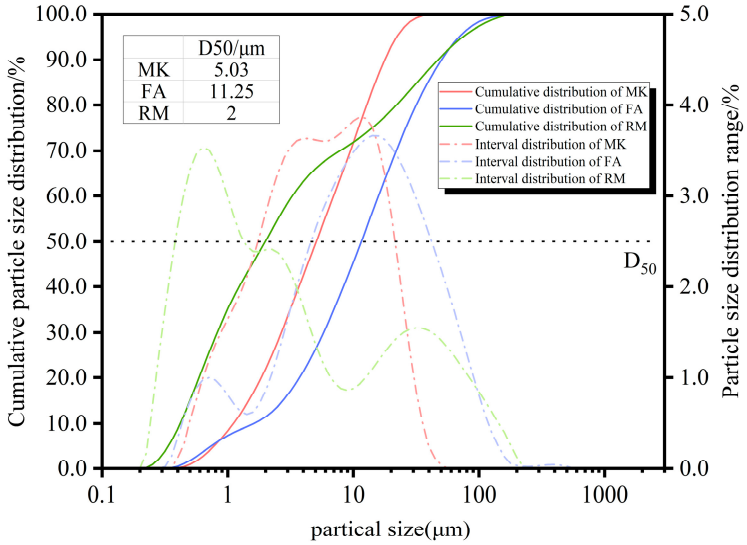


Figure 1. Particle size distributions of the precursor materials.

2.2. Ternary Mixture Design of the MK–RM–FA System

Mixture experiment design is a statistical optimization method used to evaluate the influence of component proportions on the performance of multi-component systems. Its main characteristic is that the proportions of all components are subject to a constant-sum constraint, typically equal to 100%. Unlike conventional factorial designs, which mainly examine the independent variation in different factors, mixture design focuses on the substitution and interaction effects among components within a constrained composition space. The main purpose of this method is to establish a response model for quantitatively describing the influence of component proportions on key performance indicators, to predict the performance of different formulations, and ultimately to identify the optimal mixture under specified constraints.

In this study, metakaolin (MK), fly ash (FA), and red mud (RM) were selected as the three precursor components of the ternary system. Considering both waste-utilization efficiency and environmental safety, the proportion of RM was restricted to no more than 40 wt% as an upper boundary condition. The experimental design was carried out using Design-Expert 13 software. After the composition boundaries were defined, the software automatically generated the experimental design points to form the mixture scheme shown in Table 2. Duplicate formulations included in Table 2 were retained as replicate design points to estimate experimental error and to support the statistical evaluation of model significance and lack-of-fit.

The mechanical performance of specimens prepared with different precursor proportions was systematically tested, and the relationships between component proportions and response variables were fitted using a Scheffé polynomial model. Based on this approach, response-surface analysis was used to evaluate the effects of precursor proportions and their interactions on the performance of the ternary system. This method not only reduced the experimental workload and improved testing efficiency, but also provided a scientific basis for the efficient utilization of red mud and for the proportioning of the MK–FA–RM composite precursor system. In the present study, the mixture design was primarily used for preliminary composition screening and optimization within the investigated compositional range. It should be noted that the ternary mixture design in this study was performed for the geopolymer binder system itself, without the addition of coarse aggregates. Coarse aggregates were introduced only in the subsequent preparation of water-retaining subgrade materials.

Table 2. Design matrix of the constrained ternary MK–FA–RM mixture system.

Samples	Proportion by Weight (%)		
	MK	FA	RM
A1	20	53	27
A2	100	0	0
A3	0	60	40
A4	33	53	13
A5	100	0	0
A6	50	50	0
A7	0	100	0
A8	0	80	20
A9	60	0	40
A10	60	20	20
A11	50	50	0
A12	0	60	40
A13	80	0	20
A14	35	35	30
A15	60	0	40
A16	0	100	0
A17	20	70	10

2.3. Specimen Preparation and Curing

For precursor proportion optimization, the geopolymer binder system was prepared without coarse aggregates. First, an alkaline activator with a silicate modulus of 1.7 and a Na_2O mass fraction of 16% was prepared. The activator was then mixed with the composite precursor materials of different proportions at a water-to-binder ratio of 0.5. The mixture was stirred at 600 r/min for 30 min to obtain a homogeneous geopolymer slurry, followed by low-speed stirring for an additional 5 min to eliminate residual air bubbles. The prepared slurry was cast into 40 mm × 40 mm × 40 mm molds and sealed under ambient temperature for 7 d before mechanical testing.

After the optimal precursor proportion was identified, the geopolymer slurry was further used as the binder phase for preparing water-retaining subgrade materials. In this stage, coarse aggregates of the required particle-size range were introduced and mixed until the aggregate surfaces were uniformly coated by the slurry. The resulting fresh mixture was then cast into 100 mm × 100 mm × 100 mm molds for pilot-scale specimen preparation and cured under ambient sealed conditions unless otherwise specified.

To evaluate the influence of seasonal temperature on practical preparation, pilot-scale specimens of 100 mm × 100 mm × 100 mm were produced under different environmental conditions, and the corresponding surface integrity and bonding characteristics were compared in the subsequent analysis.

2.4. Material Characterization and Performance Testing

2.4.1. Mechanical Strength Test

For precursor proportion optimization, the unconfined compressive strength (UCS) of geopolymer binder specimens without coarse aggregates was determined in accordance with JGJ/T 70-2009 using a universal testing machine (NYL-500, 300 kN, Shanghai, China) at a loading rate of 1000 N/s. The binder specimens were prepared as 40 mm × 40 mm × 40 mm cubes and cured under ambient sealed conditions for 7 d before testing. Three parallel specimens were tested for each group, and the average value was reported. For water-retaining subgrade materials containing coarse aggregates, compressive strength was measured on cubic specimens with dimensions of 100 mm × 100 mm × 100 mm using the same testing machine and loading procedure, unless otherwise specified.

For water-retaining subgrade materials containing coarse aggregates, flexural strength was measured on prismatic specimens with dimensions of 100 mm × 100 mm × 400 mm using the three-point bending method specified in JTG E51-2009 at a loading rate of 50 mm/min. Unless otherwise specified, all reported values were the average of three parallel specimens.

2.4.2. Water Retention Test

The water retention capacity, which reflects the pore structure and water-storage ability of the subgrade material, was determined using cubic specimens with dimensions of 100 mm × 100 mm × 100 mm and a total specimen volume of 1000 mL (V_t). Before testing, the specimens were dried to a constant mass. Each specimen was then placed in a graduated container, and water was slowly added until the water level reached the top surface of the specimen. The difference between the initial water level and the residual water level after specimen removal was taken as the retained water volume. The water retention rate (η) was calculated as the ratio of retained water volume to the total specimen volume. The specific test procedure was as follows: the dried specimen was placed in a transparent graduated cylinder, and clean water was slowly added until the water surface was exactly level with the top of the specimen. The corresponding water volume was recorded as the initial volume, V_i. Subsequently, the specimen was carefully removed, and the remaining water volume was recorded as V_r. Each test was performed three times, and the average value was recorded as the final result. The detailed calculation equation is shown in Equation (1):

$$\eta = 100\% \times \frac{1000 - (V_i - V_r)}{1000} \quad (1)$$

2.4.3. Water Stability and Acid Resistance

Because no directly applicable standard test method is available for this type of water-retaining subgrade material, its short-term environmental durability was evaluated by simulating natural water exposure and typical acidic corrosion conditions. After curing, the specimens were immersed for 30 d in three different media: tap water, 5% hydrochloric acid solution, and 5% sulfuric acid solution. During immersion, the liquid level was maintained above the specimen surface, and the solutions were renewed every 7 d to maintain a stable corrosive concentration. The UCS of the specimens was measured before and after immersion, and the strength retention rate was calculated to quantify the mechanical degradation under different exposure environments. This test was used to evaluate the water stability and acid resistance of the material under the investigated short-term conditions.

2.4.4. Phase Characterization

Phase composition analysis was performed by X-ray diffraction (XRD) to identify crystalline phases in the precursor materials and representative geopolymer samples. Prior to testing, the samples were dried at 105 °C for 24 h, ground, and sieved to 200–300 mesh. CaF_2 was added at a mass ratio of 2:1 as an internal standard. XRD measurements were conducted using Co Kα radiation under operating conditions of 40 kV and 40 mA. Quantitative mineralogical analysis was performed by Rietveld refinement using MAUD (version 2.999) software to identify crystalline products and evaluate phase evolution during geopolymerization. It should be noted that the mechanistic interpretation in this study is mainly based on crystalline phase evolution and compositional analysis; direct identification of Fe-bearing gel environments requires further microscopic and spectroscopic investigation.

2.5. Direct Cost Estimation Method

To scientifically evaluate the economic feasibility of the Fe-based geopolymer water-retaining subgrade material under pilot-scale preparation conditions, the direct production cost was estimated based on the 2025 market reference prices in Wuhan, China, combined with the actual mix proportions and construction requirements of the experimental scheme. In this study, the unit price method was adopted to calculate the direct engineering cost of material preparation. This method is a conventional engineering cost-estimation approach that determines the direct cost of a qualified product by summing the costs of labor, materials, and construction equipment, and is particularly suitable for pilot-scale production scenarios with clearly defined processes and standardized operating procedures.

Labor cost C_l was calculated based on labor consumption Q_l and daily wage P_l, while material cost C_m was determined from the theoretical consumption $m_{m,i}$, a material loss factor α, and unit prices $P_{m,i}$. In this study, α = 50% was adopted as a conservative loss factor for pilot-scale estimation. It should be noted that this value was used to reflect the relatively high material loss under small-batch pilot-scale preparation conditions, where slurry residue, spillage, and handling inefficiencies are more significant than in industrialized continuous production. Equipment cost C_e was calculated according to the number of machine shifts $T_{e,k}$, unit price $R_{e,k}$, and the breakdown of depreciation (D_k), maintenance (M_k), and energy (E_k) costs per rated output (N_k). The total direct unit cost C_{unit} was obtained as the ratio of total direct cost C_{direct} to the produced material volume V (Equations (2)–(8)):

$$C_{direct} = C_l + C_m + C_e \tag{2}$$

$$C_l = Q_l \times P_l \tag{3}$$

$$C_m = \sum_{i=1}^{n} (Q_{m,i} \times P_{m,i}) \tag{4}$$

$$Q_{m,i} = m_{m,i} \times (1 + \alpha) \tag{5}$$

$$C_e = \sum_{k=1}^{p} (T_{e,k} \times R_{e,k}) \tag{6}$$

$$R_{e,k} = \frac{D_k + M_k + E_k}{N_k} \tag{7}$$

$$C_{unit} = \frac{C_{direct}}{V} \tag{8}$$

2.6. Carbon Emission Analysis Method

The carbon footprint of the geopolymer water-retaining subgrade materials was evaluated following the Life Cycle Assessment (LCA) framework and the international standards ISO 14067 [15] (Carbon Footprint of Products) and EN 15804 [16] (Environmental Product Declarations for Construction Products). In accordance with standard LCA practice, industrial by-products such as fly ash (FA) and red mud (RM) were assigned zero embodied carbon, and only the emissions associated with transportation and preprocessing within the defined system boundary were considered. Therefore, the carbon-emission assessment in this study focused on four major contributors: metakaolin (MK), sodium hydroxide (NaOH), sodium silicate (Na_2SiO_3, water glass), and electricity consumption during material preparation.

The total carbon footprint CF_{total} was calculated as follows (Equation (9)):

$$CF_{total} = (M_{MK} \times EF_{MK}) + (M_{NaOH} \times EF_{NaOH}) + (M_{WG} \times EF_{WG}) + (E_E \times EF_E) \tag{9}$$

where M_i and EF_i are the mass and emission factor of component i, and E_E and EF_E represent total electricity consumption and its corresponding emission factor, respectively. The unit carbon intensity (CF_{unit}) of the final product was then determined by Equation (10):

$$CF_{unit} = \frac{CF_{total}}{M_G} \quad (10)$$

where M_G is the total mass of the produced geopolymer material. This method provides a quantitative basis for evaluating the environmental performance of the geopolymer system and enables direct comparison with conventional Portland cement-based materials under the same calculation boundary. It should be noted that the adopted zero-burden assumption for FA and RM is allocation-dependent, and different allocation approaches may result in different absolute carbon-footprint values.

3. Results and Discussion

3.1. The Influence of Iron-Containing Material Ratios in the MK-RM-FA System on the Properties of Geopolymer

To develop a suitable binder phase for water-retaining geopolymer subgrade materials, the effects of metakaolin (MK), fly ash (FA), and red mud (RM) proportions on the early-age compressive strength of the ternary precursor system were first evaluated. MK, owing to its high alkali-activation reactivity, provides sufficient reactive Si and Al species for the formation of the geopolymer gel network and thus plays a dominant role in establishing the load-bearing skeleton of the matrix. FA contributes to industrial-waste utilization and can improve particle packing and workability, but its contribution to early-age strength under ambient curing is relatively limited because of its slower dissolution rate. RM not only promotes the utilization of Fe-rich industrial residue, but may also participate in matrix stabilization through its Fe-bearing and Al-containing phases. However, excessive RM may introduce more weakly reactive or inert components and may also raise environmental and engineering concerns. Therefore, in this study, the RM content was restricted to no more than 40% to balance mechanical performance, waste utilization, and service safety [17].

To quantitatively evaluate the compositional effects, a constrained ternary mixture design was adopted, and the compressive-strength results were fitted using a linear Scheffé mixture model. Within the investigated compositional range, the fitted model showed good statistical adequacy for preliminary composition screening and optimization (Figure 2). The model was highly significant (F = 41.30, $p < 0.0001$), and the regression sum of squares accounted for 85.5% of the total variation, indicating that the mixture proportions exerted a strong influence on compressive strength. In addition, the lack-of-fit test was not significant ($p = 0.3058$), suggesting that the fitted model can adequately describe the variation trend of the experimental data within the current design space. The linear mixture model obtained for compressive strength σ_c is expressed as:

$$\sigma_c = 84.15 \times \mathrm{A} + 7.10 \times \mathrm{B} + 18.45 \times \mathrm{C}$$

where σ_c (MPa) is the 7 day compressive strength, and A, B, and C represent the mass fractions of MK, FA, and RM. Statistical analysis confirmed the model's reliability, with an F-value of 41.30 and $p < 0.0001$, indicating a highly significant effect of composition on strength. The regression explained 85.5% of total variation, and the lack-of-fit test ($p = 0.3058$) indicated strong predictive accuracy. All variance inflation factors (VIFs) were below 2, confirming the absence of severe multicollinearity and validating the robustness of the coefficients.

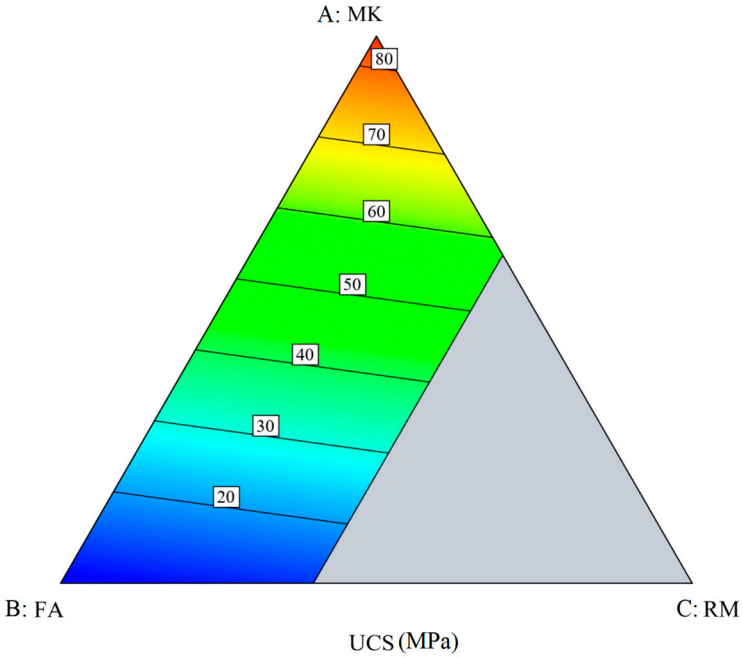


Figure 2. The results of the mixture design experiment.

The normal probability plot of residuals further confirmed the statistical reliability of the fitted model. In this study, 17 standardized residuals were ranked and converted into the corresponding normal probability percentages (Figure 3). The residuals ranged from −2.722 to 1.391, corresponding to a probability interval of 2.9% to 97.1%. The least-squares fitted line can be expressed as y = 25.83x + 50.29, where x is the standardized residual and y is the normal probability percentage. Most data points were distributed close to the fitted straight line, especially within the central probability range of 20–80%, indicating good agreement with the normality assumption. Only slight deviations were observed at the extreme ends, which did not constitute significant outliers. Overall, the residual distribution supports the validity of the normality assumption and confirms that the fitted model is statistically reliable for the present screening purpose.

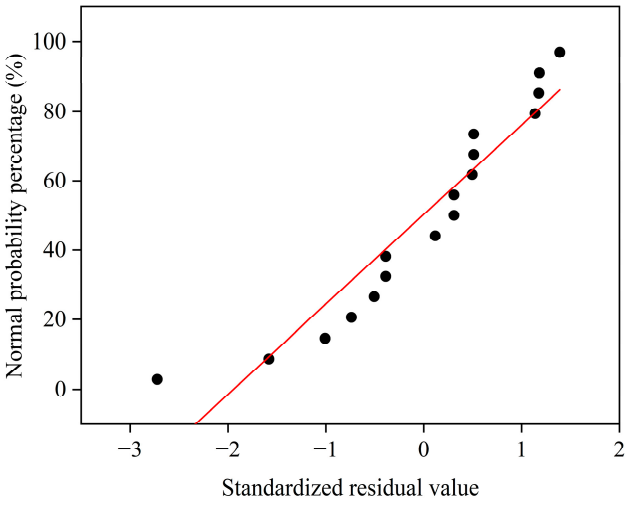


Figure 3. Normal Plot of Residuals.

The regression coefficients indicate that MK made the greatest contribution to compressive strength, followed by RM, while FA showed the smallest contribution within the present experimental range. This result is consistent with the much higher reactivity of MK

under ambient alkali activation, which enables rapid dissolution and gel formation at early ages. By contrast, although FA contains a considerable vitreous phase, its dissolution rate at room temperature is relatively low, so its role in early-age strength development is mainly associated with physical filling and delayed reactivity. RM showed a higher contribution than FA within the investigated range. This difference is consistent with the possible participation of Al- and Fe-bearing phases from RM in the reaction process, together with the physical filling effect of its fine particles. However, RM remained significantly less effective than MK, most likely because RM also contains a substantial fraction of weakly reactive or inert phases. Therefore, the positive role of RM should be interpreted within the current compositional range and should not be extrapolated to higher replacement levels without further verification.

To further clarify the relative influence of FA and RM, the fitted model was used to compare compressive-strength variation at fixed MK contents (Figure 4). The results show that, within the investigated range, increasing RM by 10% led to an increase of approximately 1.14 MPa in compressive strength, whereas increasing FA tended to suppress strength development. This opposite trend suggests that partial replacement of FA by RM is beneficial to the early-age mechanical performance of the MK–FA–RM system, provided that the RM content remains within an appropriate range.

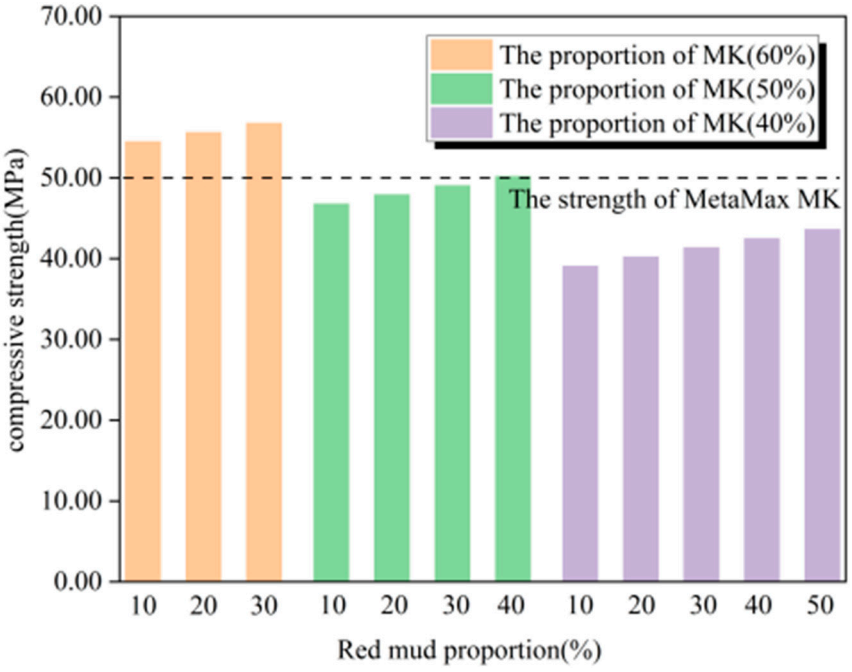


Figure 4. The influence of red mud proportion on compressive strength.

Based on the fitted model, the proportion of 60% MK, 30% RM, and 10% FA was selected as the optimal precursor composition. This selection was not based solely on the fitted compressive-strength trend, but also on the engineering relationship established in our previous study between the compressive strength of MetaMax metakaolin-based geopolymer cubes and that of water-retaining subgrade materials prepared with the same binder system. That earlier study showed that when the compressive strength of the geopolymer cube exceeded 50 MPa, the corresponding water-retaining subgrade material could satisfy the strength requirement for inorganic stabilized base materials specified in JTG D50–2017 [18]. Therefore, the 60% MK–30% RM–10% FA formulation was selected as the optimal proportion by considering both mechanical performance and economic feasibility, and was adopted in the subsequent pilot-scale preparation and performance evaluation

of the water-retaining subgrade materials. It should be noted that the compressive-strength analysis in this section was conducted on geopolymer binder specimens without coarse aggregates and was intended for precursor screening under ambient curing conditions, rather than for direct comparison with structural geopolymer concretes.

3.2. Phase Evolution and Mechanism Discussion

To clarify the origin of the different mechanical contributions of metakaolin (MK), fly ash (FA), and red mud (RM) in the ternary system, the intrinsic characteristics of the three precursor materials were first quantitatively analyzed. XRF and XRD were used to determine their major oxide compositions, phase assemblages, and Fe occurrence states. For clarity, the terms Structural Fe, Free Fe-bearing phase, and Amorphous phase content describe different characteristics of the precursor and should not be interpreted as three mutually exclusive categories. Structural Fe refers to Fe incorporated into mineral lattices or disordered solid frameworks, whereas Free Fe-bearing phase refers to Fe present as discrete Fe-rich phases such as hematite. Amorphous phase content, by contrast, describes the overall fraction of non-crystalline or poorly ordered material in the precursor. Accordingly, part of the Structural Fe may be included within the amorphous phase, whereas the Free Fe-bearing phase is generally treated as a separate crystalline or discrete Fe-rich component [19,20].

The quantitative analysis showed that RM contained a very high total Fe content of 35.82%. Although part of the Fe occurred as a Free Fe-bearing phase, a considerable fraction was present as Structural Fe associated with amorphous or weakly crystalline environments, including macaulayite, accounting for approximately 64% of the total Fe. In contrast, FA contained 13.85% Fe, of which about 85% existed as hematite, indicating that most Fe in FA was present as a Free Fe-bearing phase with relatively low reactivity. MK contained much less Fe overall, but it exhibited the highest Amorphous phase content, reaching 68.9%, which was significantly higher than those of FA (42.76%) and RM (47.36%). This high amorphous aluminosilicate fraction is consistent with the dominant role of MK in early-age geopolymer gel formation and strength development [21]. The corresponding XRD patterns and quantitative phase-analysis results are presented in Figure 5 and Table 3.

These compositional differences help explain the mechanical trends observed in Section 3.1. Under the condition of fixed MK content, increasing RM while decreasing FA led to a clear increase in compressive strength. This tendency is consistent with the different occurrence states of Fe in the two industrial residues. In RM, a larger proportion of Fe exists as Structural Fe, some of which is associated with amorphous or weakly crystalline environments and may participate, to some extent, in the dissolution–reorganization process under strong alkali activation. Such participation may facilitate the development of a more stable or more compact aluminosilicate reaction network. By contrast, the Fe in FA is predominantly present as Free Fe-bearing phases, which are less likely to participate effectively in geopolymerization and are more likely to behave as inert fillers during early-age reaction [22]. This difference provides a plausible explanation for why RM showed a higher contribution to compressive strength than FA within the investigated compositional range.

To further examine the role of RM at the local interface, SEM–EDS mapping (Figure 6) was performed on a representative reacted RM particle. The SEM image showed that the particle was not simply embedded in the matrix as an inert inclusion, but was surrounded by a relatively dense interfacial layer. The corresponding elemental maps revealed substantial spatial overlap among O, Al, Si, and Fe around the particle boundary, indicating the formation of a Si–Al–Fe-rich reaction zone. The map-sum spectrum (Table 4) of the selected region mainly contained O (62.42 wt.%), Al (8.89 wt.%), Si (9.08 wt.%), and Fe (19.61 wt.%). In particular, the interfacial region exhibited a Si/Al ratio close to 1, together with evident

Fe enrichment. This composition is consistent with the formation of Al-rich aluminosilicate reaction products, possibly including N–A–S–H/N–A–F–S–H-type gel domains around the RM particle, since Si/Al ratio is an important compositional indicator for geopolymer gel environments [21,23].

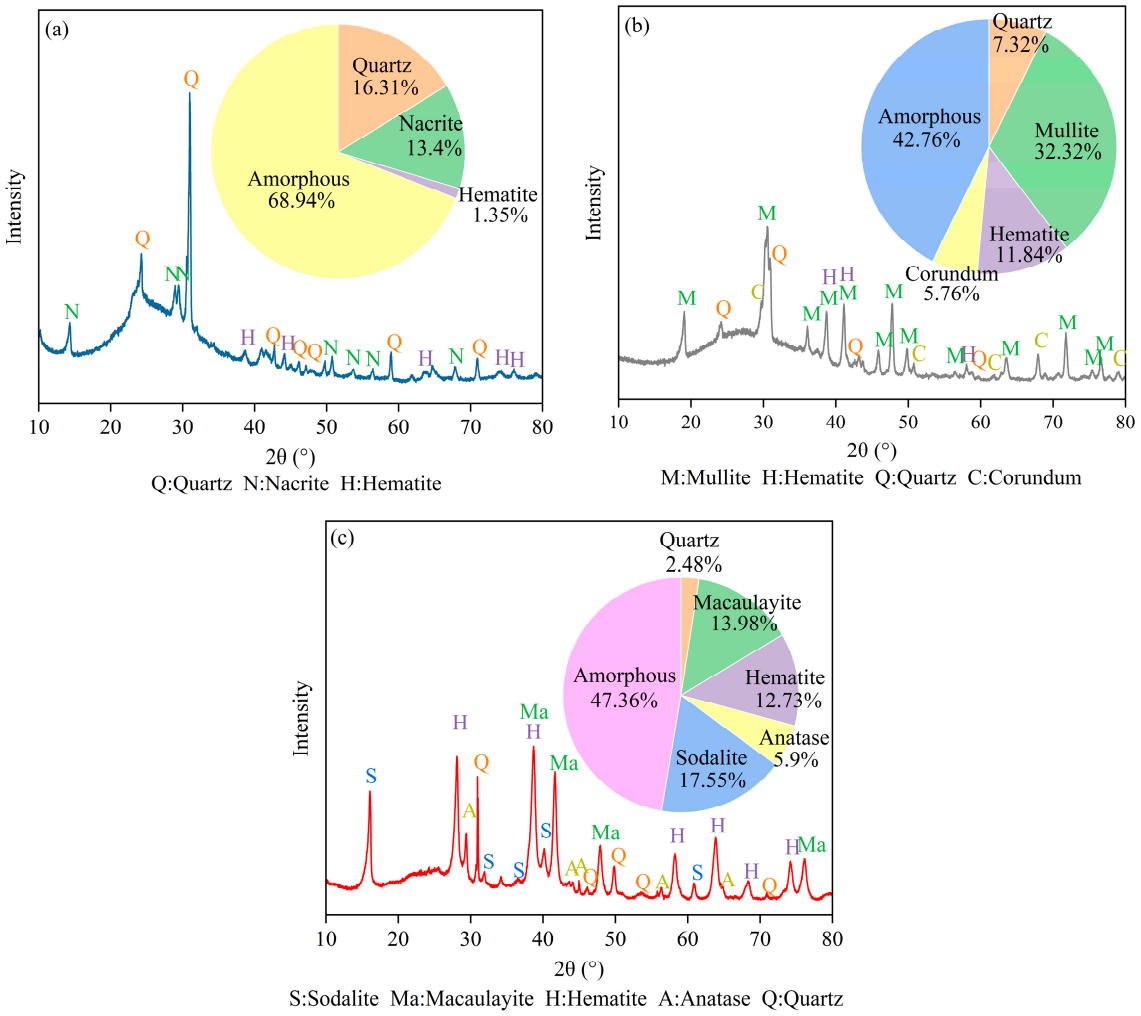


Figure 5. Quantitative XRD analysis patterns of (**a**) MK; (**b**) FA; (**c**) RM.

Table 3. The content distribution of structural iron, free Fe-bearing phase and amorphous phase components.

	Structural Fe Content (%)	Free Fe-Bearing Phase Content (%)	Amorphous Phase Content (%)
MK	0.87	1.35	68.95
FA	2.01	11.84	42.76
RM	23.09	12.73	47.36

The morphology of the reacted particle also suggests a shell-like reaction pattern, in which the outer surface of the RM particle was more strongly involved in geopolymerization, whereas part of the inner core may have remained less reacted. Similar shell-like or surface-preferential reaction features have been reported in Fe-rich or red-mud-containing alkali-activated systems, where the external layer reacts more readily than the interior under alkaline conditions [24]. This observation implies that RM did not behave as a purely inert filler in the ternary system. Instead, its outer surface appears to have undergone interfacial dissolution and reprecipitation, leading to the formation of a compact reaction

layer with good continuity to the surrounding matrix, which is consistent with the interfacial densification behavior reported for red-mud-based geopolymer systems [25,26]. Such a feature is beneficial for particle–matrix bonding and local matrix densification, and is therefore consistent with the positive contribution of RM to compressive strength within the investigated range [27].

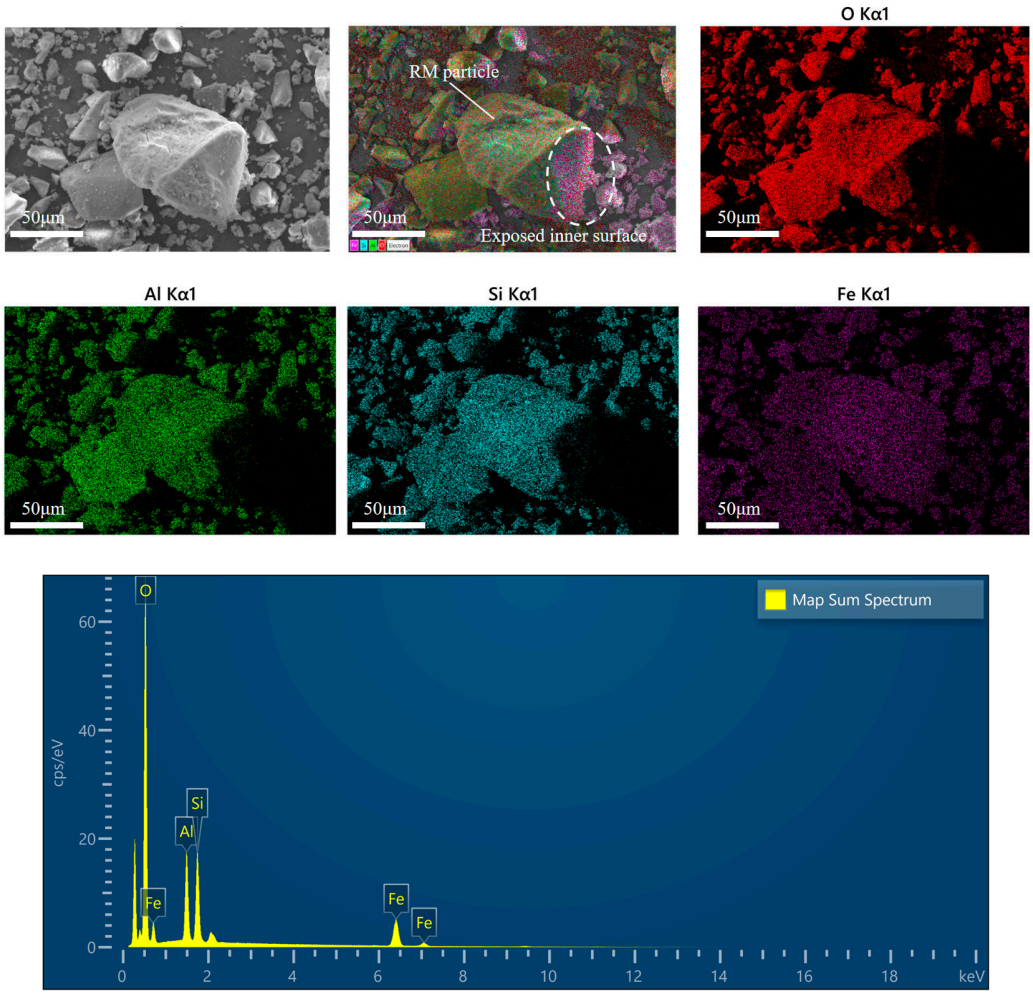


Figure 6. SEM image and EDS elemental mapping of the sample A10.

Table 4. Elemental composition of the mapped region in sample A10.

Element	Line Type	Weight/%	Sigma/%	Atomic/%
O	K series	62.42	0.12	79.54
Al	K series	8.89	0.05	6.71
Si	K series	9.08	0.05	6.59
Fe	K series	19.61	0.13	7.16

Taken together, the phase-analysis and mapping results suggest that the role of Fe-bearing precursors depends not only on total Fe content, but more importantly on the occurrence state and interfacial reactivity of Fe. Previous studies have also emphasized that the chemical state, mineral association, and local reactivity of Fe-bearing species can significantly influence geopolymer reaction pathways and the resulting microstructure, rather than total Fe content alone [28]. In the present system, Fe appears more likely to act as an interfacial modifier or network-stabilizing component within Si–Al-rich reaction products, rather than as the dominant framework-forming species, which is consistent with

recent discussions on the role of Fe in Fe-containing aluminosilicate reaction networks [19]. This interpretation also helps explain why RM, despite containing a lower Amorphous phase content than MK, still contributed more positively to strength development than FA under the investigated ambient curing conditions, whereas FA-rich systems containing a larger proportion of free hematite or other low-reactivity Fe-bearing phases often show weaker early-age contribution [29].

It should be emphasized, however, that the present mechanistic interpretation is based mainly on quantitative phase analysis, Fe occurrence-state analysis, SEM–EDS mapping, and the macroscopic strength response of the ternary system. Therefore, the results support a possible role of Fe-bearing components from RM in matrix evolution and structural stabilization, but they do not directly prove the formation of a specific Fe-bearing gel structure or the definite coexistence of distinct gel types. Similar caution has been noted in recent reviews, which point out that XRD and SEM–EDS can support phase-based or compositional interpretation but are generally insufficient, by themselves, to unambiguously identify specific gel species or Fe coordination environments [19]. In particular, although the interfacial Si/Al ratio is compatible with Al-rich N–A–S–H-type products, the mapped region contains mixed interfacial products and Fe-bearing phases, so the present EDS evidence alone cannot directly confirm a pure N–A–S–H gel; Si/Al ratio is informative for gel chemistry, but its interpretation should be combined with complementary spectroscopic evidence [21,23]. Direct identification of Fe coordination environments and Fe-modified gel domains would therefore require further spectroscopic and microscopic investigation. Nevertheless, the present results clearly indicate that the occurrence state of Fe, rather than merely its total content, is closely related to the mechanical behavior of the MK–FA–RM geopolymer system.

3.3. Effect of Aggregate Particle Size on Water Retention and Mechanical Performance

After the optimal MK–FA–RM precursor composition was determined, the influence of coarse aggregate particle size on the functional performance of the water-retaining subgrade material was further evaluated. In this system, aggregate size governs the pore structure formed between neighboring particles and therefore strongly affects both water retention capacity and load-bearing behavior. The objective of this section is not simply to maximize porosity or strength alone, but to identify an appropriate aggregate size range that can balance water-storage function with sufficient mechanical support for subgrade applications. Similar multifunctional design requirements have been emphasized in recent studies on pervious and sponge-city pavement materials, where hydraulic regulation and structural support must be considered simultaneously [14,30].

As shown in Figure 7, the water retention rate increased progressively with increasing aggregate size. The water retention rate was 25.3% for the 9.5–16.5 mm group, increased to 35.3% for the 16.5–20.0 mm group, and further rose to 42.3% for the 26.5–31.5 mm group. This trend indicates that larger aggregates tend to generate larger and more connected interparticle voids, thereby increasing the effective pore volume available for water storage. In other words, aggregate size directly regulates the storage space and connectivity of the pore system, which are key factors controlling the water retention function of the material. Similar size-dependent effects of aggregate gradation on pore connectivity, water permeability, and hydraulic performance have also been reported for porous and pervious cementitious systems [31,32].

In contrast to the improvement in water retention capacity, the mechanical properties decreased with increasing aggregate size. The compressive strength declined from 8.59 MPa for the 9.5–16.5 mm group to 8.37 MPa, 7.67 MPa, and 5.28 MPa for the 16.5–20.0 mm, 20.0–26.5 mm, and 26.5–31.5 mm groups, respectively. Flexural strength exhibited the same

tendency, decreasing from 1.70 MPa to 1.35 MPa, 0.96 MPa, and 0.51 MPa. The largest aggregate group failed to satisfy the compressive-strength requirement of 7 MPa and also fell below the minimum flexural-strength threshold of 0.9 MPa for inorganic stabilized granular materials. Therefore, although larger aggregates improved the water-storage function, they also weakened the mechanical reliability of the material. Similar inverse relationships between coarse pore development and strength have been widely reported for pervious concrete and alkali-activated porous pavement materials.

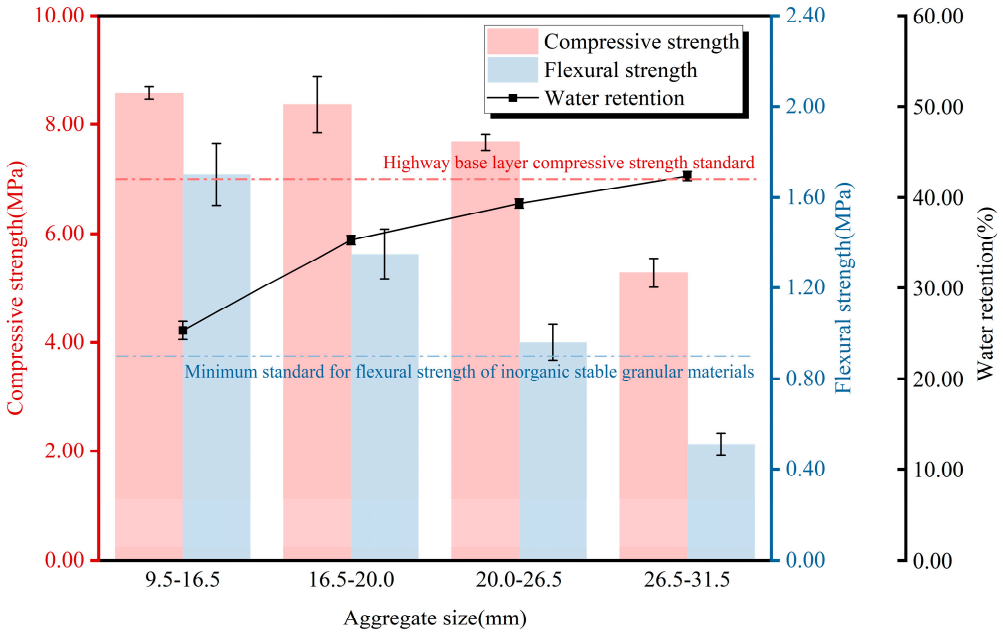


Figure 7. Water retention and mechanical performance of geopolymer subgrade materials with different aggregate size ranges.

This trade-off between water retention and strength is mainly governed by the evolution of pore structure and skeleton continuity. As the aggregate size increases, the number of contact points between adjacent particles decreases while the interparticle gaps become larger, which directly changes the geometry and connectivity of the pore network [32]. Although this favors the formation of interconnected storage voids and thus improves hydraulic functionality, coarser or gap-graded aggregate structures are also known to reduce the continuity of the load-bearing skeleton in pervious concrete systems [14]. Meanwhile, the effective binder-covered contact area becomes smaller, weakening the bridging effect of the geopolymer binder at particle contacts and making force transmission through the skeleton less uniform [30]. Under such conditions, stress is more likely to concentrate around pore boundaries and weak contact zones, which accelerates local damage development [31]. Larger interparticle pores can also reduce packing compactness and interfacial continuity, thereby promoting crack initiation and premature failure [33]. By contrast, smaller aggregate sizes tend to form a denser particle skeleton with more uniform binder distribution and stronger particle–matrix bonding, which improves compressive and flexural strength, although at the expense of water-storage space [34].

From an engineering perspective, aggregate size should therefore be selected by considering both hydraulic regulation and structural support, rather than optimizing only one function [35]. Excessively small aggregates are unfavorable for water storage because the void system becomes relatively compact and the effective storage space is restricted [36]. In contrast, excessively large aggregates can provide high water retention capacity, but this is commonly accompanied by reduced mechanical stability because the open-pore system

becomes too coarse to maintain sufficient structural integrity [37]. Among the investigated size ranges, the 16.5–20.0 mm group showed the most balanced overall performance, with a compressive strength of 8.37 MPa, a flexural strength of 1.35 MPa, and a water retention rate of 35.3%, all satisfying the relevant engineering requirements. This result is consistent with the widely reported optimization principle that intermediate aggregate gradation often provides the most favorable balance between hydraulic performance and mechanical reliability in porous pavement materials [31]. Therefore, within the investigated range and under the present mix design, 16.5–20.0 mm can be regarded as the most suitable aggregate size range for water-retaining geopolymer subgrade materials, because it provides a reasonable compromise between water-storage capacity and structural performance.

3.4. Short-Term Water Stability and Acid Resistance

Short-term durability under aqueous and acidic environments is a key performance criterion for water-retaining geopolymer subgrade materials, because the material is expected to remain in frequent contact with infiltrated water and may also be exposed to acidic species during service. In alkali-activated aluminosilicate systems, durability under immersion is closely related to the stability of the reaction products, pore connectivity, and the resistance of the interfacial structure to ion ingress and dissolution [38]. Therefore, in addition to compressive strength and water retention capacity, the resistance of the optimized material to water immersion and acid attack must be evaluated.

As shown in Figure 8, specimens soaked in tap water (Soak-W), 5% HCl (Soak-H), and 5% H_2SO_4 (Soak-S) exhibited a decrease in compressive strength compared with the unsoaked reference specimen (Soak-N), indicating that water and acidic media caused a certain degree of structural degradation. However, the degree of strength loss varied with the soaking medium. The smallest reduction was observed after tap-water immersion, whereas both acidic solutions caused more pronounced deterioration. In 5% HCl, the compressive strength decreased by an average of 9.40%, while immersion in 5% H_2SO_4 resulted in a slightly higher average loss of about 10.32%. Despite these reductions, all immersed specimens retained compressive strengths above 7.10 MPa, which still satisfied the engineering requirement for stabilized base materials specified in JTG D50–2017. These results indicate that the material maintained acceptable residual load-bearing capacity under short-term soaking conditions.

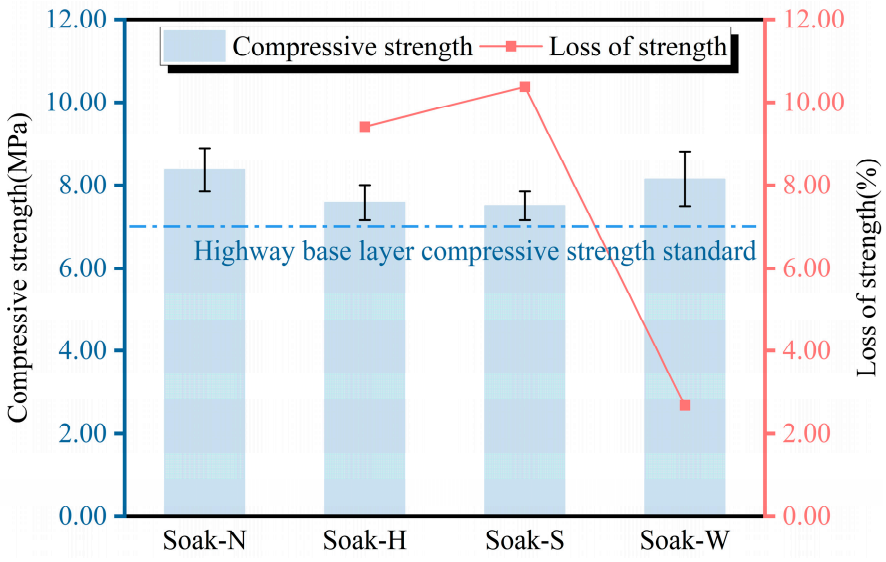


Figure 8. Compressive strength of water-retaining geopolymer subgrade materials under different soaking conditions.

Among the tested environments, the relatively limited strength loss after tap-water immersion suggests that the geopolymer matrix possessed good short-term water stability. This behavior is consistent with previous studies showing that aluminosilicate-based geopolymer systems generally maintain good stability under simple water immersion, owing to the relatively stable gel network formed during geopolymerization [39]. The observed reduction in strength under water immersion is more likely associated with limited alkali leaching, local interfacial weakening, and partial dissolution of soluble species, rather than severe destruction of the main reaction matrix.

The deterioration became more evident under acidic conditions. In 5% HCl, the moderate strength loss indicates that hydrochloric acid caused clear but still limited degradation of the geopolymer matrix. This reduction can be attributed mainly to the attack of H^+ ions on the aluminosilicate network and the progressive dissolution of charge-balancing alkali species, which may induce partial depolymerization in the outer reaction layer [40]. Nevertheless, the residual compressive strength remained above the design threshold, indicating that the material still preserved basic structural integrity under short-term hydrochloric acid exposure.

Immersion in 5% H_2SO_4 produced the greatest strength loss among the tested conditions, showing that sulfuric acid was more aggressive than hydrochloric acid in the present system. In addition to proton attack, sulfate-containing solutions may intensify deterioration through coupled dissolution and surface damage, leading to more severe weakening of the exposed region than that caused by HCl alone [41]. Even so, the difference in strength loss between the two acidic environments remained limited, suggesting that the optimized MK–FA–RM binder system still maintained a relatively stable reaction matrix during short-term exposure.

Overall, the results show that the developed material possesses satisfactory short-term environmental durability for water-retaining subgrade applications. Although all soaking conditions caused some reduction in compressive strength, the residual strengths remained above the engineering requirement, and the material exhibited particularly good stability under tap-water immersion. The more pronounced deterioration in sulfuric acid indicates that acidic environments, especially sulfate-containing ones, deserve greater attention in long-term service evaluation. Therefore, while the present results support the short-term applicability of the material in water-retaining roadbed systems, further study under prolonged chemical exposure and cyclic wetting–drying conditions is still necessary.

3.5. Pilot-Scale Preparation and Seasonal Applicability

To verify the engineering feasibility of the optimized material beyond the laboratory scale, pilot-scale preparation was carried out using the selected MK–FA–RM precursor composition and aggregate size range. Two field-oriented pilot sections were constructed under representative summer and winter conditions, each with dimensions of 3 m × 5 m × 0.5 m. The winter trial was conducted at an ambient temperature of 0–5 °C, whereas the summer trial was performed at 30–40 °C. To ensure that the mechanical test results could more realistically reflect the performance of the in situ material, specimens were prepared by synchronous pouring using the same batch of mixture, placement procedure, and compaction method as those adopted in the pilot sections. Compared with conventional laboratory specimens, this approach provided a more direct basis for evaluating field construction applicability.

The mechanical results showed that the system was highly sensitive to the construction season. As shown in Figure 9, the summer-prepared specimens S1–S3 achieved compressive strengths of 9.8, 9.5, and 10.5 MPa, respectively, corresponding to an average of 9.93 MPa. Their flexural strengths were 1.5, 1.4, and 1.8 MPa, respectively, with an average of 1.57 MPa. By contrast, the winter-prepared specimens W4–W6 exhibited compressive

strengths of only 2.9, 3.5, and 2.5 MPa, while all three specimens showed flexural strengths of merely 0.3 MPa. These results indicate that both compressive and flexural performance were markedly reduced under winter preparation conditions, demonstrating that near-freezing temperatures severely suppressed early-age strength development at the pilot scale. This observation is consistent with previous studies reporting that low-temperature curing significantly delays the development of mechanical properties in metakaolin-based geopolymers and geopolymer-stabilized systems [42,43].

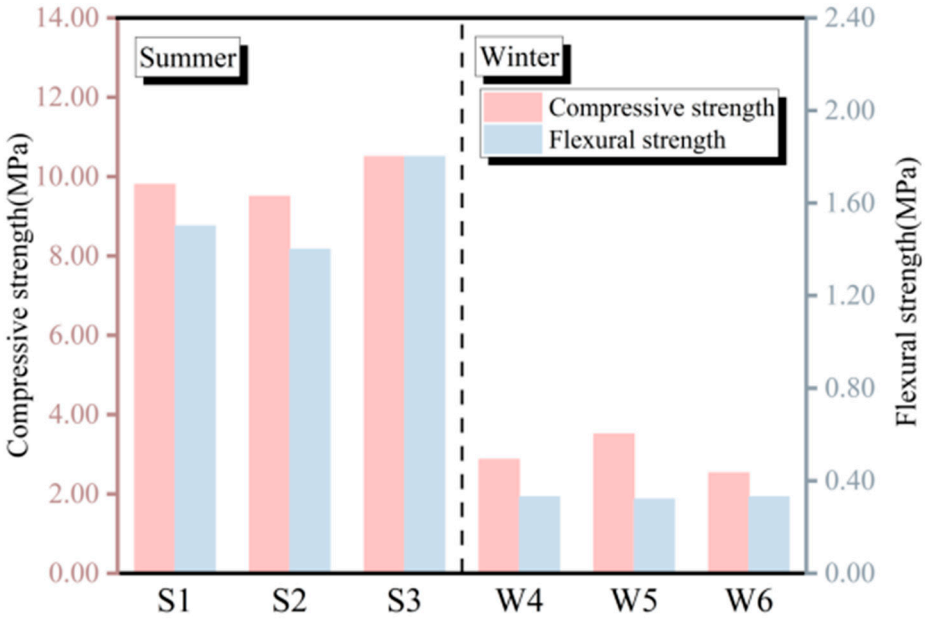


Figure 9. Mechanical properties of pilot-scale water-retaining geopolymer subgrade specimens prepared in summer and winter.

The above performance differences can be attributed mainly to the strong temperature sensitivity of geopolymerization and interfacial evolution. Elevated ambient temperature accelerates the dissolution of reactive aluminosilicate species and promotes gel formation and polycondensation, thereby facilitating the rapid establishment of a continuous binding network and a dense matrix structure [43]. At the same time, warm conditions improve the rheological evolution of metakaolin-based geopolymer pastes, enabling the binder to more effectively wet and coat aggregate surfaces during mixing and placement. In contrast, under winter low-temperature conditions, reduced ion mobility and slower dissolution–condensation processes delay gel formation and hinder the development of the interfacial transition zone. As a result, the binder cannot fully encapsulate the aggregates before structural stiffening and moisture loss occur, making the material more susceptible to shrinkage cracking, interfacial debonding, and strength deficiency. The surface morphology shown in Figure 10 is fully consistent with this interpretation: the summer samples exhibited continuous encapsulation and a relatively dense structure, whereas the winter samples showed severe cracking and discontinuous bonding. Previous reviews have likewise emphasized that curing regime and thermal environment are critical variables governing early geopolymer network formation and construction applicability [19,23].

From an engineering perspective, the pilot-scale results indicate that the optimized MK–FA–RM system has good construction potential under warm-season conditions, whereas its field applicability is highly sensitive to ambient temperature. Considering the severe deterioration observed in the winter pilot trial (0–5 °C), together with previous studies showing that low-temperature curing markedly suppresses metakaolin-based geopolymerization and early strength development [44], it is recommended that the mini-

mum ambient temperature for direct field construction of this material should be controlled above 10 °C. When the ambient temperature falls within 5–10 °C, auxiliary measures such as thermal insulation, preheating, or enclosed curing should be adopted. Direct construction below 5 °C is not recommended. Overall, the pilot-scale study demonstrates that construction season is a key factor controlling the practical applicability of the developed material and should be explicitly considered in future field implementation and construction specifications.

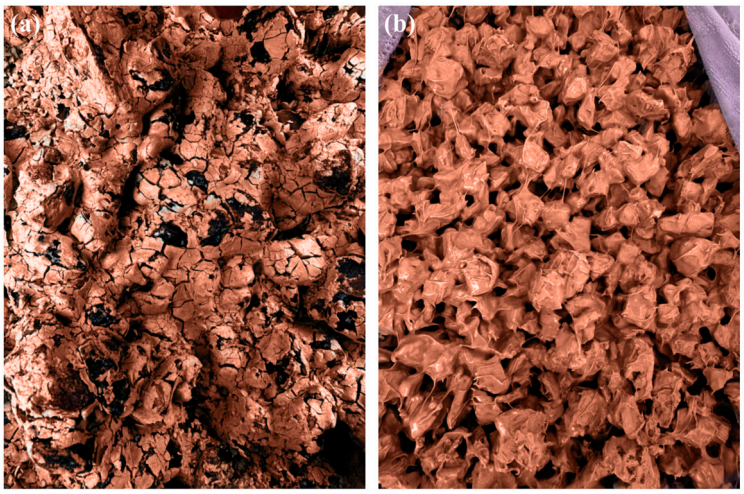


Figure 10. Surface appearance of pilot-scale water-retaining geopolymer subgrade specimens after 7 days of curing: (**a**) winter and (**b**) summer.

3.6. Economic and Carbon-Emission Assessment

A pilot-scale cost evaluation was conducted to assess the economic feasibility of iron-based geopolymer water-retaining subgrade materials and to identify the primary cost drivers in production (Table 5). The optimized ternary system consisted of MK, FA, and RM as cementitious precursors, activated by sodium hydroxide and sodium silicate (modulus 2.25), with crushed aggregates incorporated to form a stable skeleton. Material loss during production was approximately 50%, and mixing and curing water were also considered in the calculation. For benchmarking (Table 6), a MetaMax-based geopolymer system was prepared under the same production conditions. In that system, each 10 × 10 × 10 cm block contained 65 g of MetaMax, 111 g of sodium silicate, 3.2 g of sodium hydroxide, 14 g of water, and 800 g of coarse aggregate. The total production volume was about 7.5 m^3, which was considered sufficient to simulate practical engineering conditions.

Table 5. Estimated direct engineering cost of ternary geopolymer water-retaining subgrade materials.

	Unit Price (¥)	Count	Cost (¥)
MK	8/kg	519 kg	4152
FA	4.8/kg	87 kg	417.6
RM	5.5/kg	259 kg	1424.5
Sodium hydroxide	2.5/kg	73 kg	182.5
Sodium silicate	3/kg	435 kg	1305
Aggregate	0.17/kg	6000 kg	1020
Cost of labor	250/d	5 d	1250
Water utility cost	3.5/t	0.3 t	1.05
Electricity cost	0.6/kWh	20 kWh	12
Total	-	-	9752.65

Table 6. Estimated direct engineering cost of MetaMax-based geopolymer water-retaining subgrade materials.

	Unit Price (¥)	Count	Cost (¥)
MetaMax MK	20.8/kg	488 kg	10,150.4
Sodium hydroxide	2.5/kg	24 kg	60
Sodium silicate	3/kg	833 kg	2499
Aggregate	0.17/kg	6000 kg	1020
Cost of labor	250/d	5 d	1250
Water utility cost	3.5/t	0.42 t	1.47
Electricity cost	0.6/kWh	20 kWh	12
Total	-	-	14,992.87

Equipment costs were relatively minor and mainly included a flat-mouth mixer and a PE mixing barrel, with a total purchase cost of ¥1930. Assuming a 5% residual value, a service life of 3000 production cycles, and an electricity consumption of 20 kWh per shift, the equipment-related cost was estimated to be approximately ¥3.06/m^3. Labor expenses were calculated based on the local construction wage of ¥250/day. A total of five worker-days were required for material preparation, mixing, transport, casting, and curing, resulting in a labor cost of ¥1250. Water costs were negligible, amounting to only ¥1.05 for 0.3 tons of water consumed. In contrast, material cost was the dominant component of the overall expenditure. For the ternary system, 2025 Wuhan market data indicated a total material cost of ¥8502, accounting for 87% of the total direct cost, among which metakaolin and red mud together contributed ¥5576.5, corresponding to 57.2% of the total cost. In comparison, the MetaMax-based system showed a much stronger dependence on high-purity metakaolin, which alone accounted for 67.8% of the total cost. This is consistent with previous studies identifying high-reactivity aluminosilicate precursors as one of the principal cost drivers in geopolymer production. In comparison, the MetaMax-based mix showed a significantly higher reliance on high-purity metakaolin, which alone represented 67.8% of the total cost, consistent with prior studies identifying high-reactivity aluminosilicate precursors as the principal cost driver in geopolymer production. The total cost of the ternary geopolymer material was approximately ¥9752.65, equivalent to ¥1300/m^3, with materials contributing ~¥1133/m^3—roughly 61% of the cost of MetaMax-based materials—while labor represented 12.8% and other factors were negligible. These findings confirm that raw material inputs overwhelmingly determine production costs, yet the use of industrial by-products such as fly ash and red mud can substantially reduce expenditure without compromising performance. From an engineering perspective, high-grade precursors like metakaolin remain indispensable for achieving superior compressive strength, impermeability, and durability, and although their unit cost is higher, life-cycle assessments demonstrate that these materials can offset initial expenses through extended service life and reduced maintenance requirements. Labor costs in the pilot-scale study were relatively elevated due to the absence of mechanization, but future automated and continuous production processes are expected to significantly lower labor input and improve cost-efficiency. Overall, the analysis demonstrates both the technical and economic feasibility of ternary iron-based geopolymers as sustainable alternatives for water-retaining roadbed construction.

The transition toward large-scale utilization of industrial by-products such as fly ash and red mud offers significant opportunities to optimize the cost structure and enhance the sustainability of iron-based geopolymer water-retaining roadbed materials. In the current pilot-scale production, these materials are still purchased as raw materials, contributing ¥1842.1, or 18.9% of the total cost. However, with the development of regional solid waste co-processing systems and policies promoting resource recovery, these by-products could be sourced directly from local power and alumina plants, reducing procurement costs and

limiting expenses to transportation and minimal pretreatment. Under such a scenario, the total production cost could be reduced by ¥2449.5, decreasing from ¥9752.65 to ¥7303 and lowering the unit cost from ¥1302/m^3 to ¥974/m^3, representing a 25% cost reduction. This aligns with international findings that the use of industrial waste-based geopolymers can reduce raw material costs by 20–30% compared with conventional systems.

Beyond economic benefits, the large-scale utilization of fly ash and red mud also provides substantial environmental advantages. By replacing virgin raw materials and reducing landfill disposal, this strategy can mitigate greenhouse gas emissions, reduce leachate and heavy-metal pollution risks, and lower the ecological burden associated with waste stockpiling. Previous life-cycle assessment studies have consistently shown that geopolymer systems incorporating industrial by-products exhibit a markedly lower carbon footprint than Portland cement-based materials. From a broader sustainability perspective, this approach also aligns well with China's "zero-waste city" strategy and current policy directions concerning solid-waste pollution prevention and resource utilization. Nevertheless, the variability in the composition, mineralogy, and reactivity of industrial waste streams means that a stable supply chain and quality-control system are still essential to ensure consistent field performance. Overall, the synergistic use of industrial by-products in iron-based geopolymers offers clear potential for cost reduction, environmental protection, and engineering promotion, making these materials promising candidates for large-scale application in sustainable infrastructure construction. A life-cycle carbon emission analysis was conducted for the pilot-scale production of approximately 6.2 t of iron-based geopolymer water-retaining roadbed material, comprising 519 kg metakaolin, 87 kg fly ash, 259 kg red mud, 73 kg sodium hydroxide, 435 kg sodium silicate, 6000 kg coarse aggregate, and 218 kg water. The assessment focused on three primary stages: metakaolin calcination, alkaline activator production, and electricity consumption during mixing, curing, and early-age maintenance. The emission factor for metakaolin was set at 0.40 kg CO_2-e/kg based on reported values for dehydroxylation at ~850 °C. Sodium hydroxide, produced through energy-intensive membrane electrolysis, was assigned a factor of 5.8 kg CO_2-e/kg, while sodium silicate was estimated at 1.5 kg CO_2-e/kg. Electricity-related emissions were calculated using the 2025 Central China Grid average of 0.7 kg CO_2-e/kWh [45].

The results (Figure 11) show that the total carbon footprint of the geopolymer system is approximately 210 kg CO_2-e/t—about 70–75% lower than conventional CEM I cement concrete (800–900 kg CO_2-e/t)—demonstrating the significant emission reduction potential of alkali-activated materials and industrial by-product utilization. Emission partitioning reveals that sodium silicate is the largest contributor (50.3%), followed by sodium hydroxide (32.6%), metakaolin calcination (16%), and electricity consumption (1.1%). These results align with previous LCA findings that alkaline activators dominate geopolymer carbon emissions, highlighting the need for targeted mitigation strategies.

Two approaches can further reduce emissions: (i) optimizing activator formulations, for example by partially replacing sodium hydroxide or sodium silicate with lower-carbon alternatives such as sodium carbonate or recycled silica sol; and (ii) adopting alternative heat sources—including industrial waste heat, solar thermal energy, or biomass gasification—for metakaolin production. Future large-scale production scenarios that integrate locally sourced fly ash and red mud with renewable electricity or carbon capture technologies could potentially reduce total emissions to around 150 kg CO_2-e/t, offering substantial carbon savings relative to Portland cement-based systems. These findings provide robust quantitative evidence for the low-carbon potential of iron-based geopolymer roadbed materials and support their adoption in sustainable infrastructure applications, including sponge city drainage systems, ecological slope protection, and stormwater retention projects.

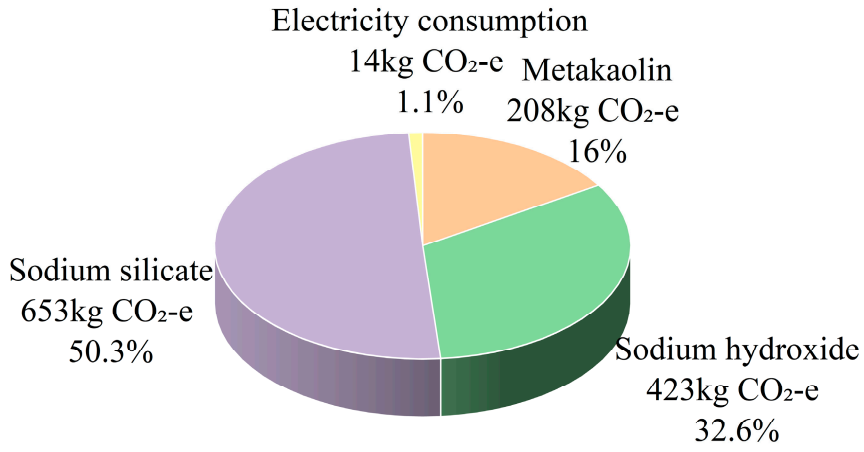


Figure 11. Carbon-emission analysis of pilot-scale water-retaining geopolymer subgrade materials.

4. Conclusions

In this study, an Fe-based geopolymer water-retaining subgrade material was developed based on a ternary precursor system of metakaolin (MK), fly ash (FA), and red mud (RM). Through precursor optimization, phase and microstructural characterization, aggregate-size regulation, durability evaluation, pilot-scale verification, and economic and carbon-emission assessment, its engineering applicability was systematically investigated. The main conclusions are as follows:

1. The precursor composition had a decisive effect on strength development. Within the investigated range, MK contributed most to compressive strength, FA showed a relatively limited contribution, and RM performed more favorably than FA under the tested conditions. Considering strength, waste utilization, and engineering applicability, the optimal precursor composition was determined to be 60% MK, 10% FA, and 30% RM.
2. The different roles of MK, FA, and RM were closely related to their amorphous contents, Fe occurrence states, and interfacial reactivity. MK provided the dominant reactive aluminosilicate source for gel formation, whereas RM was more favorable than FA for matrix evolution and local interfacial stabilization. SEM–EDS mapping further suggested that RM did not merely act as an inert filler, but likely participated in reacted-matrix development to some extent.
3. Aggregate particle size controlled the balance between water retention capacity and mechanical performance. Increasing aggregate size improved pore connectivity and water retention capacity, but also reduced skeleton continuity and particle–matrix bonding, leading to lower strengths. Among the investigated size ranges, 16.5–20.0 mm showed the best overall balance, with a compressive strength of 8.37 MPa, a flexural strength of 1.35 MPa, and a water retention rate of 35.3%.
4. The optimized material showed acceptable short-term durability, but its practical applicability was highly temperature-dependent. After soaking in tap water, 5% HCl, and 5% H_2SO_4, all specimens retained strengths above the engineering threshold, although strength losses were observed in all environments. Pilot-scale preparation further showed that summer conditions were favorable, whereas winter preparation at 0–5 °C caused severe cracking and substantial strength loss. A minimum ambient construction temperature of 10 °C is therefore recommended for direct field application.
5. The ternary iron-based geopolymer system showed clear engineering potential from both economic and environmental perspectives. The direct cost of the optimized ternary material was approximately ¥1300/m^3, substantially lower than that of the MetaMax-based reference system, while its total carbon footprint was about 210 kg

H_2SO_4, much lower than that of conventional Portland cement-based materials. These results confirm that the synergistic use of MK, FA, and RM can achieve a favorable balance among engineering performance, industrial solid-waste utilization, economic feasibility, and carbon reduction.

Future work should focus on long-term field monitoring, coupled durability under wetting–drying and chemical exposure, and further reduction in activator-related cost and carbon emissions. In addition, construction guidelines for different seasonal conditions and more locally available low-carbon activator systems should be developed to support large-scale application.

Author Contributions: X.W.: Writing—original draft, Conceptualization, Writing—review and editing, Supervision, Methodology. Z.C.: Methodology, Formal analysis. X.Z.: Writing—review & editing, Supervision, Funding acquisition. Y.X.: Writing—review & editing, Investigation, Funding acquisition. Z.H.: Visualization, Methodology. Z.F.: Writing—review & editing, Visualization, Funding acquisition. All authors have read and agreed to the published version of the manuscript.

Funding: This research was funded by the National Natural Science Foundation of China (51978536 and 52300147) and the Research Project of China Three Gorges Corporation (0704230).

Data Availability Statement: The original contributions presented in this study are included in the article. Further inquiries can be directed to the corresponding authors.

Acknowledgments: The authors gratefully acknowledge the contributions of all staff involved in field sampling, experiments, data processing, and information gathering for this project.

Conflicts of Interest: Authors Xian Wu and Yinhang Xu were employed by the company Wuhan Municipal Engineering Design & Research Institute Co., Ltd. Wuhan, Hubei, 430023, China. The remaining authors declare that the research was conducted in the absence of any commercial or financial relationships that could be construed as a potential conflict of interest.

References

1. Abiodun, Y.O.; Olanrewaju, O.A.; Gbenebor, O.P.; Ochulor, E.F.; Obasa, D.V.; Adeosun, S.O. Cutting Cement Industry CO_2 Emissions through Metakaolin Use in Construction. *Atmosphere* **2022**, *13*, 1494. [CrossRef]
2. Bheel, N.; Awoyera, P.; Tafsirojjaman, T.; Sor, N.H.; Sohu, S. Synergic effect of metakaolin and groundnut shell ash on the behavior of fly ash-based self-compacting geopolymer concrete. *Constr. Build. Mater.* **2021**, *311*, 125327. [CrossRef]
3. Jindal, B.B.; Alomayri, T.; Hasan, A.; Kaze, C.R. Geopolymer concrete with metakaolin for sustainability: A comprehensive review on raw material's properties, synthesis, performance, and potential application. *Env. Sci. Pollut. Res. Int.* **2023**, *30*, 25299–25324. [CrossRef]
4. Jingliang, D.; Zhen, T.; Xiaopeng, S.; Changjie, X.; Yan, Z.; Hao, W.; Jun, H.; Sui, X.; Changming, L.; Tingting, Z. Development of sustainable alkali activated red mud composite cement: Mechanical properties, hydration mechanisms, and environmental benefits. *Constr. Build. Mater.* **2025**, *499*, 144089. [CrossRef]
5. Kumar, A.; Saravanan, T.J.; Bisht, K.; Kabeer, K.I.S.A. A review on the utilization of red mud for the production of geopolymer and alkali activated concrete. *Constr. Build. Mater.* **2021**, *302*, 124170. [CrossRef]
6. Ai, T.; Zhong, D.; Zhang, Y.; Zong, J.; Yan, X.; Niu, Y. The Effect of Red Mud Content on the Compressive Strength of Geopolymers under Different Curing Systems. *Buildings* **2021**, *11*, 298. [CrossRef]
7. Raj, R.; Yadav, B.; Yadav, J.S.; Kumar, S. Advancement in soil stabilisation process by utilising fly ash-red mud geopolymer: A comprehensive review. *Discov. Mater.* **2025**, *5*, 216. [CrossRef]
8. Dixit, A.; Das, S.K. Fly ash stabilised red mud as a one-part alkali-activated sustainable material for pavement subgrade: Strength, durability and life cycle assessment analysis. *Road Mater. Pavement Des.* **2025**, *26*, 2536–2562. [CrossRef]
9. Sun, H.; Xie, X.; Xie, M.; Pu, H. Development of geopolymer with red mud, fly ash, calcium carbide slag, and phosphogypsum as a step toward low-carbon building materials. *Waste Manag.* **2026**, *215*, 115436. [CrossRef] [PubMed]
10. Xu, L.-Y.; Lao, J.-C.; Qian, L.-P.; Shi, D.-D.; Lan, J.; Xie, T.-Y.; Hou, D.; Huang, B.-T. Upcycling red mud into high-strength high-ductility Engineered Geopolymer Composites (EGC): Toward superior performance and sustainability. *Compos. Part B Eng.* **2025**, *305*, 112713. [CrossRef]
11. Joumblat, R.; Al-Smaily, A.A.M.; de Medeiros Melo Neto, O.; Youssef, A.M.; Soliman, M.R. Cooling and Hydrological Performance of Porous Asphalt Pavements: A State-of-the-Art Review for Urban Climate Resilience. *Sustainability* **2026**, *18*, 3836. [CrossRef]

12. Huang, Y.; Sun, H.; Liu, Y.; Zhao, K.; Liu, T.; Liu, D. Application of pervious concrete pavement in the "breathe in-breathe out" design for sponge cities in China. *Environ. Sci. Pollut. Res.* **2024**, *31*, 40818–40837. [CrossRef]
13. Lu, Q.; Sha, A.; Chen, Y.; Ren, X.; Wang, S.; Wu, J.; Jiao, W. Mechanical and thermal performance of semi-flexible pavement incorporating foam concrete grout. *Constr. Build. Mater.* **2025**, *495*, 143691. [CrossRef]
14. Wu, Y.; López-Carreño, R.-D.; Aidarov, S.; Álvarez, P.P. Pervious concrete pavements for climate change adaptation and mitigation: A systematic review of performance, sustainability, and future perspectives. *Road Mater. Pavement Des.* **2025**, 1–36. [CrossRef]
15. *ISO 14067:2018*; Greenhouse Gases—Carbon Footprint of Products—Requirements and Guidelines for Quantification. International Organization for Standardization: Geneva, Switzerland, 2018.
16. *EN 15804:2012+A2:2019*; Sustainability of Construction Works—Environmental Product Declarations—Core Rules for the Product Category of Construction Products. European Committee for Standardization: Brussels, Belgium, 2019.
17. Cui, W.; Liu, J.; Duan, W.; Xie, M.; Li, X.; Dong, X. Study on the synergistic effects and eco-friendly performance of red mud-based quaternary cementitious materials. *Constr. Build. Mater.* **2024**, *428*, 136352. [CrossRef]
18. Cao, R.; Fang, Z.; Shang, Y. Production of a New Base Material for Load-Bearing Water-Storing Road. *J. Mater. Civ. Eng.* **2022**, *34*, 04022144. [CrossRef]
19. Kumar, S.G.K.M.; Kinuthia, J.M.; Oti, J.; Adeleke, B.O. Geopolymer Chemistry and Composition: A Comprehensive Review of Synthesis, Reaction Mechanisms, and Material Properties-Oriented with Sustainable Construction. *Materials* **2025**, *18*, 3823. [CrossRef]
20. Liu, W.; Wang, S.; Zhang, T.; Zhu, H.; Chang, N.; Zhang, L.; Hu, Z. A Review of Preparation of Low-Carbon Cementitious Materials from Chemically Activated Red Mud: Synergy, Hydration Mechanism, Rheological Properties and Applications. *Langmuir* **2025**, *41*, 15735–15751. [CrossRef]
21. Liu, Y.; Bi, C.; Gao, Y.; Gyakari, F.N.; Zha, X. Role of Reactive Silica Addition in Enhancing Geopolymerization Efficiency and Strength Development of Calcined Granite Waste. *Materials* **2026**, *19*, 886. [CrossRef]
22. Abas, K.M.; Ngida, R.E.A.; Abbas, S.M. Impact of reinforcement additives on physical and electrical properties of fly ash-based geopolymer materials. *Sci. Rep.* **2026**, *16*, 12207. [CrossRef] [PubMed]
23. Ricciotti, L.; Lucariello, D.; Perrotta, V.; Apicella, A.R. Aversa, Sustainable Alkali-Activated and Geopolymer Materials: What Is the Future for Italy? *Recycling* **2025**, *10*, 140. [CrossRef]
24. Li, Z.; Xu, Y.; Wu, C.; Zhang, W.; Chen, Y.; Li, Y. Preparation and Research on Mechanical Properties of Eco-Friendly Geopolymer Grouting Cementitious Materials Based on Industrial Solid Wastes. *Materials* **2024**, *17*, 3874. [CrossRef] [PubMed]
25. Wang, X.; Xue, Y. Preparation and Immobilization Mechanism of Red Mud/Steel Slag-Based Geopolymers for Solidifying/Stabilizing Pb-Contaminated Soil. *Materials* **2024**, *17*, 3353. [CrossRef]
26. Zhao, J.; Yu, G.; Hu, L.; Dong, Y.; Liu, H.; Guo, C.; Wang, Y. Mechanical Properties of Basalt–Polypropylene Hybrid Fiber-Reinforced Red Mud–Coal Metakaolin Geopolymer. *Materials* **2026**, *19*, 1578. [CrossRef]
27. Chakkor, O. Durability and Mechanical Analysis of Basalt Fiber Reinforced Metakaolin–Red Mud-Based Geopolymer Composites. *Buildings* **2025**, *15*, 2010. [CrossRef]
28. Fang, Y.; Zhuang, K.; Cui, H.; Zhang, Z.; Wang, A.; Wang, C.; Zheng, D.; Wang, X. The state of Fe^{3+} in the C–F–A–S–H system with varying Fe/Si and Ca/Si ratios. *J. Mater. Chem. A* **2023**, *11*, 26193–26211. [CrossRef]
29. Kozub, B. Properties of Geopolymers Based on Fly Ash with the Addition of Asphalt from Road Surface Demolition. *Materials* **2025**, *18*, 4488. [CrossRef]
30. Azad, A.; Sheikh, M.N.; Hai, F.I. Design of alkali-activated pervious concrete for pavement applications: Impact of contents and chemical compositions of binders. *Eur. J. Environ. Civ. Eng.* **2026**, *30*, 1–27. [CrossRef]
31. Bui, P.-H.; Doan, C.-C.; Tran, V.-K.; Huynh, T.-P. Experimental evaluation of the effect of aggregate gradation on strength gain and drainage ability of pervious concrete. *Int. J. Pavement Eng.* **2026**, *27*, 2634954. [CrossRef]
32. Wijekoon, S.H.B.; Sathiparan, N.; Subramaniam, D.N. Optimisation of pervious concrete performance by varying aggregate shape, size, aggregate-to-cement ratio, and compaction effort by using the Taguchi method. *Int. J. Pavement Eng.* **2024**, *25*, 2380523. [CrossRef]
33. Fu, J.; Jiang, L.; Yang, M.; Yu, D.; Shen, M.; Wang, Y. Influence of Nano-Silica and Porosity on the Strength and Permeability of Permeable Concrete: An Experimental Study. *Buildings* **2026**, *16*, 148. [CrossRef]
34. Fan, X.; Liu, S.; Li, Y.; Liu, H.; Wang, J. Synergistic Enhancement of Mechanical Strength and Permeability in Hybrid Fiber-Reinforced Pervious Concrete: Experimental Characterization and Multiscale Pore Structure Analysis. *J. Mater. Civ. Eng.* **2026**, *38*, 04026143. [CrossRef]
35. Khong, S.C.; Yee, J.J.; Tee, K.F.; Chin, S.C. Permeable concrete: Current state-of-the-art and perspectives. *Innov. Infrastruct. Solut.* **2024**, *9*, 427. [CrossRef]
36. Bai, X.; Zhou, H.; Bian, X.; Chen, X.; Ren, C. Compressive Strength, Permeability, and Abrasion Resistance of Pervious Concrete Incorporating Recycled Aggregate. *Sustainability* **2024**, *16*, 4063. [CrossRef]

37. Zhou, Z.; Yang, Z.; Cheng, S.; Yang, L. Performance of pervious concrete prepared using alkali-activated slag and recycled concrete aggregates. *Case Stud. Constr. Mater.* **2026**, *24*, e06057. [CrossRef]
38. Haddaji, Y.; Majdoubi, H.; Tayeh, B.; Akkouri, N.; Alimrani, N.; Qamouche, K. Multi-Environmental Durability of Geopolymer Composites: Mechanisms of Degradation and Performance Enhancement. *Int. J. Pavement Res. Technol.* **2026**, 1–26. [CrossRef]
39. Ekinci, E.; Kantarcı, F.; Maraş, M.M.; Ekinci, E.; Türkmen, İ.; Demirboğa, R. Historiography, Current Practice and Future Perspectives: A Critical Review of Geopolymer Binders. *Sustainability* **2025**, *17*, 9204. [CrossRef]
40. Amala, M.; Fathima, M.H.; Vignesh, R.; Karuppasamy, S.; Umarani, C. Multi-Objective Optimization and Durability Enhancement of Self-Compacting Geopolymer Concrete Using Industrial By-Products. *Iran. J. Sci. Technol. Trans. Civ. Eng.* **2026**. [CrossRef]
41. Abdulmatin, A.; Dueramae, S.; Benchaphong, A.; Thongraksa, A.; Pethrung, S. Compressive Strength and Acid Resistance of Fly Ash Based One-Part Geopolymer. *Civ. Eng. J.* **2026**, *12*, 774–784. [CrossRef]
42. Liu, F.; Luo, H.; Wan, X. Experimental study of the mechanical and thermal properties of metakaolin based geopolymer stabilized soil during low temperature curing. *Cold Reg. Sci. Technol.* **2024**, *218*, 104085. [CrossRef]
43. Lopes, A.; Lopes, S.; Pinto, I. Influence of Curing Temperature on the Strength of a Metakaolin-Based Geopolymer. *Materials* **2023**, *16*, 7460. [CrossRef] [PubMed]
44. Liu, Y.; Zhang, J.; Fan, Y.; Ge, C.; Feng, C. Improved freeze–thaw resistance and mechanical properties of engineered geopolymer composites with silica fume. *Mater. Struct.* **2026**, *59*, 127. [CrossRef]
45. Wang, F.; Zhao, S.; Sun, Y.; Song, G.; Sun, Y.; Zhao, K.; Liu, R.; Li, Y.-Y. Strategies optimization to improve environmental benefit of chicken manure anaerobic digestion in China: Insight from life cycle assessment. *J. Clean. Prod.* **2025**, *508*, 145589. [CrossRef]

Disclaimer/Publisher's Note: The statements, opinions and data contained in all publications are solely those of the individual author(s) and contributor(s) and not of MDPI and/or the editor(s). MDPI and/or the editor(s) disclaim responsibility for any injury to people or property resulting from any ideas, methods, instructions or products referred to in the content.